

# Hyperdimensional Feature Fusion for Out-Of-Distribution Detection

Samuel Wilson, Niko Sünderhauf, Feras Dayoub  
Queensland University of Technology\*

{s84.wilson,niko.suenderhauf,feras.dayoub}@qut.edu.au

## Abstract

We introduce powerful ideas from Hyperdimensional Computing into the challenging field of Out-of-Distribution (OOD) detection. In contrast to most existing work that performs OOD detection based on only a single layer of a neural network, we use similarity-preserving semi-orthogonal projection matrices to project the feature maps from multiple layers into a common vector space. By repeatedly applying the bundling operation  $\oplus$ , we create expressive class-specific descriptor vectors for all in-distribution classes. At test time, a simple and efficient cosine similarity calculation between descriptor vectors consistently identifies OOD samples with better performance than the current state-of-the-art. We show that the hyperdimensional fusion of multiple network layers is critical to achieve best general performance.

## 1. Introduction

Deep Neural Networks can achieve excellent performance on many vision tasks when the distribution of training data closely matches the test data. However, this assumption is often violated during deployment: especially in embodied AI application domains such as robotics and autonomous systems, objects and scenes that were not part of the training data distribution will inevitably be encountered. When confronted with such out-of-distribution (OOD) samples, deep neural networks tend to fail silently, producing overconfident but erroneous predictions [11] that can pose severe risks [43]. It is therefore critically important that OOD samples are identified effectively during deployment.

Previous techniques for OOD detection used softmax probabilities [13, 22] or distances in logit space [12] to distinguish in-distribution (ID) from out-of-distribution samples, making the implicit assumption that the features of a *single* layer in a Deep Neural Network (DNN) contain suf-

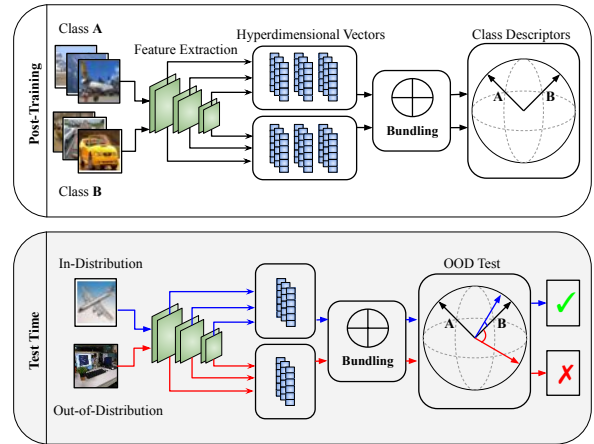


Figure 1: Illustration of our HDFS OOD detector. **Top:** After training, we extract the feature maps of in-distribution classes from multiple layers of the DNN and project them into a new hyperdimensional space with a similarity-preserving projection matrix. Using the bundling operation  $\oplus$  we create class-specific hyperdimensional descriptor vectors. **Bottom:** During testing, we repeat feature extraction, projection and bundling to obtain a hyperdimensional image descriptor. OOD samples will produce descriptors with a large angular distance to all class descriptors (red vector).

ficient information to identify OOD data. However, deeper layers of a DNN can be more sensitive to OOD samples than the softmax probabilities [35], which are often overconfident in the presence of OOD samples [11]. Recent work investigating the utility of the features from *multiple* layers in a DNN found that creating models of in-distribution classes from raw features is impractical without first reducing the number of dimensions [35, 21, 33] due to the curse of dimensionality [50].

In this paper, we introduce the powerful concepts of similarity-preserving projection and bundling from Hyper Dimensional Computing (HDC) [42] to OOD detection. Figure 1 provides a high-level description of our proposed OOD detector. We project the feature maps from *multiple*

\*The authors acknowledge continued support from the Queensland University of Technology (QUT) through the Centre for Robotics. We also thank Peer Neubert from Chemnitz University of Technology for greatly insightful discussions on the topic of Hyperdimensional Computing.

layers of a network into a common high-dimensional vector space, using similarity-preserving semi-orthogonal projection matrices. This allows us to effectively *fuse* the information contained in multiple layers: a series of *bundling* operations  $\oplus$  creates a class-specific high-dimensional vector representation for each of the in-distribution classes from the training dataset. During testing, we use the same principles of projection and bundling to obtain a single vector representation for a new input image. OOD samples can then be efficiently identified through cosine similarity operations with the class-specific representations.

Our Hyperdimensional Feature Fusion (HDFF) approach relies on the pseudo-random nature of its projection matrices and the similarity-preserving properties of the bundling operation  $\oplus$  to effectively fuse information contained in the feature maps across multiple layers in a deep network. HDFF avoids the difficulties of estimating densities in high-dimensional spaces [35, 21], removes the limitation of relying on a single layer [13, 12], does not require to select informative layers based on example OOD data [15, 47, 23], and does not rely on expensive sampling techniques (such as ensembles [19] or Monte Carlo Dropout [6]) to identify OOD samples. HDFF can be applied to a trained network and does not require re-training or fine-tuning. Our HDFF detector achieves a new state-of-the-art performance for OOD detection in conjunction with networks trained with standard cross-entropy loss or more sophisticated logit space shaping approaches [48].

In summary, our contributions are the following:

1. We propose a novel OOD detector based on the principles of Hyperdimensional Computing and achieve new state-of-the-art performance on common OOD detection benchmarks.
2. We show that fusing features from multiple layers is critical for general OOD detection performance, as different layers vary in sensitivity to different OOD data, but fusion results in OOD performance that is approximately on par or even better than the best single layer.
3. We show that our hyperdimensional feature fusion approach achieves consistent performance across a wide range of values for hyperparameters such as the number of dimensions of the hyperdimensional space and the cosine distance decision threshold.

## 2. Related Work

Out-of-distribution (OOD) detection has been addressed in the context of image classification [22, 23, 48, 13] and semantic segmentation [12, 5, 1, 2] with a diverse set of solutions to each of the problems. Many approaches try to extrapolate the properties of the distribution of OOD data by utilising a small subset of the data to fine-tune on. When

this information is unavailable, distances or densities in the softmax probabilities and logit spaces are used. Comparatively few bodies of work exist that use multiple feature maps for OOD detection. We highlight the overarching concepts and most relevant contributions below.

**OOD Fine-tuning** Some prior work [39, 15, 47, 23, 22, 5, 1] requires the availability of an OOD dataset to train or fine-tune the network or adjust the OOD detection process. However, such approaches are problematic. By definition, the OOD dataset has to always be incomplete: during deployment, samples that do not match the assumptions embedded in the OOD dataset can still be encountered, leaving such methods exposed to high OOD risk. In contrast, we do not require prior knowledge about the characteristics of OOD data.

**OOD Agnostic** Most approaches that do not rely on the availability of OOD data during training or validation analyse the model outputs to identify OOD data during deployment. Early work [13] showed the maximum of a model’s softmax output to be a good baseline. Expanding on this idea, [12] proposed using the maximum of the unnormalised output logits. Additional methods focus on extracting more information from the outputs [32] or learning calibrated confidence estimates [4, 20]. Model averaging techniques such as Deep Ensembles [19], Monte Carlo (MC) Dropout [6, 12] and SWA-G [25, 48] often improve the OOD detection performance. Training networks with specialised losses that impose a beneficial structure on the feature space has been growing in popularity recently [26, 48, 27]. E.g. the recent 1D Subspaces [48] OOD estimator encourages the network to learn orthogonal features in the layer before the logits. The approaches discussed above attempt OOD detection based on only a *single* layer in the network. In contrast, we show that utilising *multiple* layers is very beneficial for OOD detection.

**Multi-Feature OOD Detection** Newer approaches incorporate and analyse multi-scale feature maps extracted from a DNN to detect OOD samples. The use of feature maps and additional information extracted from a network has been shown to set a new state-of-the-art in OOD segmentation [5, 1] when used as input to an auxiliary OOD detection network. The requirement on an auxiliary network necessarily entails training on OOD data in the OOD detection task, but in the related field of online performance monitoring we see similar methods demonstrate failure case detection without knowledge of the types of failures to be encountered [37, 38]. Avoiding these problems altogether, recent works have tried to model in-distribution classes without an auxiliary network [35, 21, 33]. However, the curse of dimensionality requires these methods to rely on PCA reductions [35, 21] or random projections [33], losing information from the feature maps. The existing approaches to using feature maps from across the network rely on ei-

ther training an auxiliary network on OOD data or reducing the feature maps to model the training data. By contrast we use techniques from HDC to model our in-distribution data without the need for an auxiliary network. We seek to build upon initial suggestions from [35] that different layers in a DNN are more sensitive to input perturbations than softmax probabilities.

### 3. Hyperdimensional Computing

Hyperdimensional Computing (HDC), also known as Vector Symbolic Architectures, is the field of computation with vectors in hyperdimensional, very large, spaces. HDC techniques leverage the large amount of expressive power in the hyperdimensional (HD) space to model associations between data points using redundant HD vector encodings. Redundant means that in spaces of  $10^4$  dimensionality it can be seen that two random vectors are almost guaranteed to be within 5 degrees of orthogonal [41] known as *quasi-orthogonality*. The associations between data points are represented as vectors, and the set of the representative vectors is known as the *associative memory* [9]. Construction of the associative memory is done through the structure combination of HD vectors using a set of standard operations. For our application we are primarily interested in the *bundling*  $\oplus$  and *binding*  $\otimes$  operations. We also make note of the requirement for *encoding* of lower dimensional representations into a target HD space.

**Bundling** The bundling  $\oplus$  operation is used to store a representation of multiple input vectors that retains similarity to all of the input vectors [34]. Concretely, given random vectors  $\mathbf{a}$ ,  $\mathbf{b}$  and  $\mathbf{c}$ , the vector  $\mathbf{a}$  will be similar to the bundles  $\mathbf{a} \oplus \mathbf{b}$ ,  $\mathbf{a} \oplus \mathbf{c}$  and  $\mathbf{a} \oplus \mathbf{b} \oplus \mathbf{c}$ , although in the final case it will be less similar as the bundled vector needs to be similar to all 3 input vectors. Typically, the bundling operation is implemented as element-wise addition with some form of normalisation to the required space for the architecture [41]. Normalisation steps that are commonly seen are normalisation to a magnitude of one [10, 7] or cutting/thresholding to a range of desired values [8]. Without normalisation, the bundling operation is commutative and associative; when normalisation steps are added the associative aspect of the operation is approximate,  $(\mathbf{a} \oplus \mathbf{b}) \oplus \mathbf{c} \approx \mathbf{a} \oplus (\mathbf{b} \oplus \mathbf{c})$  [41].

**Binding** The binding  $\otimes$  operation is used to combine a set of vectors into one representation that is dissimilar to all of the input vectors [34]. Given the quasi-orthogonality property of HD spaces, this entails that in all likelihood, the binding operation will generate a vector orthogonal to all of the input vectors in the cosine similarity space. The second core trait of the binding operation is that it approximately preserves the similarity of two vectors before and after binding if they are bound to the same target vector. More precisely, for a set of vectors in the same hyperdimensional space  $\mathbf{a}$ ,  $\mathbf{b}$  and  $\mathbf{c}$ , that  $sim(\mathbf{a}, \mathbf{b}) \approx sim(\mathbf{a} \otimes \mathbf{c}, \mathbf{b} \otimes \mathbf{c})$ .

**Encoding** The format of the original data will not always be in the hyperdimensional space that is required. Encoding addresses this by projecting each data point from the original space into the new HD space. The selection of data encoding into a HD space depends on the type of the original data [36, 14]. An important principle of encoding is that distances in the input are preserved in the output [14], much like the binding operation. Examples of encoding include multiplication with a projection matrix [28], fractional binding [17] that preserves real numbered differences, or the encoding proposed in [14] that preserves similarities of vectors over time and spatial coordinates.

We provided only a brief introduction to HDC, for more in-depth discussions and comparisons between known architectures we encourage the reader to consider [41, 30, 16].

### 4. Hyperdimensional Feature Fusion

We propose Hyperdimensional Feature Fusion (HDF), a novel Out-of-Distribution detection method that applies the HDC concepts of Encoding and Bundling to the features from *multiple* layers in a deep neural network, and does not require re-training or fine-tuning. Our core idea is to project the feature maps from multiple layers into a common vector space, using similarity-preserving semi-orthogonal projection matrices. Through a series of bundling operations, we create a class-specific vector-shaped representation for each of the classes in the training dataset. During deployment, we repeat the projection and bundling steps for a new input image, and use the cosine similarity to the class representatives to identify OOD samples.

**Preliminaries** From a pretrained network  $f$ , we can extract feature maps  $\mathbf{m}_l$  from different layers  $l \in \{1, \dots, L\}$  in the the network. We apply an average pooling operation across the spatial dimensions to reduce the tensor-shaped (height  $\times$  width  $\times$  channels) feature maps to vector representations  $\mathbf{v}_l$  for each layer. Since the feature maps of different layers have a different number of channels  $c_l$ , we have to project the vectors  $\mathbf{v}_l$  into a common  $m$ -dimensional vector space  $\mathbb{R}^m$  in order to combine them. Conventional sizes for HD spaces range on of  $10^3 - 10^4$  [31, 28, 14], meaning that typically our HD space will be much larger than our original space  $m \gg c$ .

**Feature Encoding** Any  $m \times c$  matrix  $\mathbf{P}$  projects a  $c$ -dimensional vector  $\mathbf{v}$  into a  $m$ -dimensional space by left-multiplying:  $\mathbf{P}\mathbf{v}$ . However, preserving the cosine similarity of the projected vectors is a crucial consideration for our application in OOD detection. We therefore impose that the projection matrices  $\mathbf{P}_l$  preserve the inner product of any two vectors  $\mathbf{a}$  and  $\mathbf{b}$  in their original and their projected vector spaces. Formally, this means that

$$(\mathbf{P} \cdot \mathbf{a})^T \cdot (\mathbf{P} \cdot \mathbf{b}) = \mathbf{a}^T \cdot \mathbf{b} \quad (1)$$

$$\mathbf{a}^T \cdot \mathbf{P}^T \cdot \mathbf{P} \cdot \mathbf{b} = \mathbf{a}^T \cdot \mathbf{b} \quad (2)$$

Above condition is satisfied by any matrix that fulfils the requirement  $\mathbf{P}^\top \mathbf{P} = \mathbf{I}$ , which is the defining property of a semi-orthogonal matrix. Using the approach of [40], we therefore create a unique, pseudo-random, semi-orthogonal projection matrix  $\mathbf{P}_l$  for each of the considered layers  $l$ . These project the feature vectors  $\mathbf{v}_l$  into a common  $m$ -dimensional vector space:

$$\mathbf{h}_l = \mathbf{P}_l \mathbf{v}_l \quad \text{so that } \mathbf{h}_l \in \mathbb{R}^m \quad \forall l \in \{1, \dots, L\} \quad (3)$$

**Feature Bundling** Following the previous steps, we obtain a set of  $L$  high-dimensional vectors  $\mathbf{h}_l^{(i)}$  for an input image  $\mathbf{x}^{(i)}$ . Since all  $\mathbf{h}_l^{(i)}$  are elements of the same vector space, we can use the bundling operation  $\oplus$  to combine them into a single vector  $\mathbf{y}^{(i)}$  that serves as an expressive descriptor for the input image  $\mathbf{x}^{(i)}$ :

$$\mathbf{y}^{(i)} = \bigoplus_{l=1}^L \mathbf{h}_l^{(i)} = \bigoplus_{l=1}^L \mathbf{P}_l \cdot \mathbf{v}_l^{(i)} \quad (4)$$

As explained in Section 3, the resulting vector  $\mathbf{y}^{(i)}$  will be cosine-similar to all contributing vectors  $\mathbf{h}_l^{(i)}$ , but dissimilar to vectors from  $\mathbb{R}^m$  that were not part of the bundle. Essentially,  $\mathbf{y}^{(i)}$  provides a summary of the feature vectors  $\mathbf{v}_l^{(i)}$  of the entire network for a single image  $\mathbf{x}^{(i)}$ .

By bundling the descriptors of all images from the training set belonging to class  $c$ , we obtain a class-specific descriptor  $\mathbf{d}_c$ :

$$\mathbf{d}_c = \bigoplus_{j \in \mathbb{I}_c} \mathbf{y}^{(j)} \quad (5)$$

where  $\mathbb{I}_c$  denotes the set of indices of the training images belonging to class  $c$ .

The bundling operation  $\oplus$  can be implemented in various ways, as we discussed in Section 3. We implement  $\oplus$  to be an element-wise sum, without truncation.

**Out-of-Distribution Detection** During testing or deployment, an image  $\mathbf{x}$  can be identified as OOD by obtaining its image descriptor  $\mathbf{y}$  according to (4), and calculating the cosine similarity to each of the class-specific descriptors  $\mathbf{d}_c$ . Let  $\theta$  be the angle to the class descriptor  $\mathbf{d}_c$  that is most similar to  $\mathbf{y}$

$$\theta = \min_c \cos^{-1} \left( \frac{\mathbf{y}^\top \mathbf{d}_c}{\|\mathbf{y}\| \cdot \|\mathbf{d}_c\|} \right), \quad c \in \{1, \dots, C\} \quad (6)$$

The input  $\mathbf{x}$  is then treated as OOD if  $\theta$  is bigger than a threshold parameter:  $\theta > \theta^*$ .

## 5. Experiments

We conduct a series of experiments to demonstrate the efficacy of Hyperdimensional Feature Fusion for OOD detection. Following established evaluation protocols, we

achieve new state-of-the-art results. We furthermore report the results of a number of ablation studies, investigating the influence of the dimensionality of the hyperdimensional space, which layers are most sensitive to OOD data, and how sensitive our method is to the decision parameter  $\theta^*$  during deployment.

### 5.1. Methodology

**Datasets** Following the established evaluation protocol [48, 22], we use CIFAR10 and CIFAR100 [18] as the in-distribution datasets, using the standard 50,000 images for training. We base our evaluation on two OOD datasets: **TinyImageNet (TIN)**, which consists of 10,000 images at a resolution of 36x36 belonging to 200 classes sampled from the ImageNet dataset [3]; and the **LSUN** [46] test set which consists of 10,000 images of scenes divided into 10 classes at varying resolutions. We use the four sets of OOD images proposed by [22]<sup>1</sup> that were generated by applying a random crop (LSUNc and TINc) or random resize (LSUNr and TINr) transformation.

**Evaluation Metrics** We use the standard metrics [48, 22] to evaluate our OOD detection performance. **AUROC**: The Area Under The Receiver Operating Characteristic curve corresponds to the area under the ROC curve with true positive rate (TPR) on the y-axis and false positive rate (FPR) on the x-axis. AUROC can be interpreted as the probability that an OOD sample will be given a higher score than an ID sample [12]. **FPR95**: The FPR95 metric reports the FPR at a critical threshold which achieves a minimum of 95% in TPR. **AUPR**: The Area Under Precision Recall curve (AUPR) metrics are calculated as the area under the precision-recall curve. In the following evaluations we use two AUPR measures; **AUPR-Out** where OOD samples are given the positive label and raw OOD scores are used, and **AUPR-In** where ID samples are labelled as the positive class and OOD scores are inverted (multiplied by -1). **Detection Error**: Detection Error indicates the minimum misclassification probability with respect to the critical threshold. **F1**: F1-score corresponds to the harmonic mean of precision and recall. Since F1-score is calculated on a static binarisation determined by the critical threshold  $\theta^*$ , comparisons between methods are made on the best F1-score over all critical threshold values. The comparison to previous work according to the F1-score is done in isolation from the other metrics as some previous works only reported F1-score.

We provide additional analysis of the overlap and distances between ID and OOD datasets, for this, we consider two additional metrics. Firstly, the **Battacharyya Coefficient** gives us an approximation of the area of overlap between two distributions, lower coefficients mean less over-

<sup>1</sup>Download links for OOD datasets can be found in the following repository: <https://github.com/facebookresearch/odin>

lap between the distributions. Secondly, **Kullback-Leibler (KL) Divergence** measure that differences between two distributions, higher divergence means the two distributions are less similar. Calculation of most metrics is done through the TorchMetrics library [44].

**Implementation** We follow the evaluation procedure defined in [48, 22], implementing the standard WideResNet [49] network with a depth of 28 and a width of 10. For the evaluation, we train this network with the standard cross-entropy loss (referred to as CE-model), and with a slightly modified version of the 1D subspace approach from [48] (referred to as 1DS-Model). Our modifications to the 1DS-Model are the unfreezing of the weights and biases of the last layer during training. We do this because we find this modification results in an improvement on the evaluation metrics for the original Spectral Discrepancy detector [48] over default re-runs of the publicly available code<sup>2</sup>.

When applying HDFF to the networks we hook into the output of the BasicBlock components of the WideResNet architecture. This application means a total of 12 hooks will be applied and the same number of semi-orthogonal projection matrices  $\mathbf{P}$  will be generated.

While most of the existing OOD methods are single-inference methods, others apply multiple inference passes, e.g. using Monte Carlo Dropout [6]. When comparing against these multi-inference methods, we apply MC Dropout to obtain the approximate probability that an input  $\mathbf{x}^{(i)}$  is OOD as

$$p(\theta^{(i)} > \theta^* | \mathbf{x}^{(i)}) \approx \frac{1}{S} \sum_{n=1}^S \mathbb{I}(\theta_n^{(i)} > \theta^*) \quad (7)$$

where  $\mathbb{I}$  is the indicator function, returning 1 (OOD) when  $\theta_n^{(i)} > \theta^*$  or 0 otherwise, and  $\theta_n^{(i)}$  is obtained according to (6) for the  $n$ -th of  $S$  samples. All of our ablations in Section 5.3 are evaluated in the single-inference pass setting.

Unless otherwise stated, we operate in a hyperdimensional space of  $10^4$  dimensions. We ablate this hyperparameter in Section 5.3.2. Before projecting feature maps into the hyperdimensional space as per (5), we apply mean-centering by subtracting the layer-wise mean activations (obtained from the training set) from all  $\mathbf{m}_l$ .

**Baselines** We compare against the standard baselines defined in [48]. In the comparison with AUROC and related metrics we use the softmax prediction [13] and OLTR [24] baselines. For the F1-score setting we additionally add in the Counterfactual [29] and CROSR [45] baselines. For additional evaluation we compare the Max Logit [12] detector and extend upon the public code for the Spectral Discrepancy [48] detectors using the CE- and 1DS-Models respectively. Re-implemented methods will be marked with a dagger <sup>†</sup> in relevant tables. Since the modifications we apply to

the 1DS-Model produce results exceeding re-runs of publicly available code in the single-inference pass setting, we evaluate against this better performing model in the interest of fairness. The published results of the Spectral Discrepancy [48] detector only report results for the 50 MC sample setting. To extract results and report the additional metrics required for comparison we re-run their public code but add necessary modifications to fit into our pipeline (substitute Numpy functions for Torch functions), we do not fundamentally change the OOD detection pipeline. We use Dropout sampling [6] to collect samples in the multi-inference pass setting for the methods we re-implement.

## 5.2. Results and Discussion

Table 1 compares the results of our HDFF OOD detector to other methods across the majority of the metrics. Across the board, our HDFF detector captures OOD samples with higher fidelity than all other competing baselines. We see that the HDFF-enabled models from both training methodologies in the single-inference pass setting compete or exceed the results of the strong methods that utilise 50 MC samples, with the incorporation of MC sampling in our case increasing the gap. The results clearly show that the applying the principles of HDC to leverage the power of multiple layers throughout the network is greatly beneficial to OOD detection performance.

Table 2 compares the results with additional recent OOD detection techniques in terms of the F1-score metric. Congruent with the findings from Table 1, the addition of the HDFF detector improves the binarisation capabilities of the network as well. In many cases, we see that same behaviour as before, HDFF-enabled networks in the single-inference pass setting competes with or exceeds methods requiring 50 MC samples. Interestingly, whilst the variable threshold metrics on LSUNc in the CIFAR100 + 50 MC samples setting are slightly lower than the Spectral Discrepancy detector [48], we note that on both F1-score and FPR@95 HDFF performs better, indicating that binarised performance is overall better for HDFF.

Figure 2 visualises the differences in distributions of angular distance between the ID and OOD datasets in the CIFAR10 setting through a KDE estimate (for smoothing) over binned angular distances. We compare the distributions between Spectral Discrepancy, Figure 2a, and HDFF, Figure 2b, on the same 1D Subspaces trained model. Both figures show that in general OOD data is mapped away from the training data in a meaningful way, however only the HDFF detector shows consistent behaviour in the mapping of OOD data. Specifically, we see that the HDFF detector maps the nearly all of OOD data into the region of 50 - 65 degrees away from the nearest class descriptors. This behaviour is more desirable than the uniform distribution given in Figure 2a, as it displays a set of standard character-

<sup>2</sup>Code can be found at <https://github.com/zaemzadeh/OOD>

ID set	OOD set	FPR@95 ↓	Detection Error ↓	AUROC ↑	AUPR-In ↑	AUPR-Out ↑
		Softmax Pred (Standard) [13]/OLTR (Other) [24]/Spectral Disc <sup>†</sup> (1D Subspaces)[48]/ HDFF (1D Subspaces)/ HDFF (Standard)				
CIFAR10	TINc	38.9/25.6/13.8/ <b>4.0/3.4</b>	21.9/14.8/9.4/ <b>4.2/3.9</b>	92.9/91.3/95.9/ <b>99.2/99.2</b>	92.5/93.2/96.8/ <b>99.3/99.3</b>	91.9/88.3/95.0/ <b>99.2/98.9</b>
	TINr	45.6/28.8/11.6/ <b>3.5/6.3</b>	25.3/15.8/8.2/ <b>4.0/5.6</b>	91.0/90.3/97.5/ <b>99.4/98.7</b>	89.7/92.3/97.8/ <b>99.4/98.8</b>	89.9/87.1/97.4/ <b>99.4/98.7</b>
	LSUNc	35.0/21.3/11.5/ <b>2.9/5.3</b>	20.0/13.0/8.1/ <b>3.6/4.9</b>	94.5/92.9/97.2/ <b>99.3/98.6</b>	95.1/94.4/97.6/ <b>99.4/98.9</b>	93.1/90.8/97.0/ <b>99.2/98.1</b>
	LSUNr	35.0/21.7/9.5/ <b>2.0/3.8</b>	20.0/13.2/7.1/ <b>2.9/4.3</b>	93.9/92.6/98.1/ <b>99.7/99.1</b>	93.8/94.4/98.3/ <b>99.7/99.2</b>	92.8/90.0/98.0/ <b>99.7/99.0</b>
CIFAR100	TINc	66.6/63.8/44.2/ <b>26.2/27.7</b>	35.8/29.0/22.7/ <b>12.7/13.3</b>	82.0/77.4/85.8/ <b>95.0/94.0</b>	83.3/78.7/87.9/ <b>95.4/94.4</b>	80.2/74.4/83.5/ <b>95.0/93.4</b>
	TINr	79.2/72.9/45.7/ <b>27.4/20.2</b>	42.1/32.1/23.6/ <b>11.0/10.4</b>	72.2/73.1/85.7/ <b>95.8/96.2</b>	70.4/73.8/87.4/ <b>95.6/96.2</b>	70.8/69.8/84.7/ <b>96.2/96.3</b>
	LSUNc	74.0/59.2/48.4/ <b>33.6/62.6</b>	39.5/29.5/24.3/ <b>17.1/30.0</b>	80.3/76.9/83.9/ <b>91.4/77.9</b>	83.4/80.0/86.2/ <b>92.4/80.0</b>	77.0/72.9/81.3/ <b>90.4/75.7</b>
	LSUNr	82.2/61.9/41.0/ <b>25.0/20.9</b>	43.6/29.2/21.9/ <b>9.8/10.9</b>	73.9/77.0/87.4/ <b>96.5/95.6</b>	75.7/79.2/89.2/ <b>96.5/95.5</b>	70.1/73.3/86.4/ <b>96.7/96.0</b>
MC Sampling Methods (50 Samples)						
Max Logit <sup>†</sup> (Standard) [12]/Spectral Disc (1D Subspaces)[48]/ HDFF (1D Subspaces)/ HDFF (Standard)						
CIFAR10	TINc	13.3/9.0/ <b>3.0/3.4</b>	8.7/6.8/ <b>3.7/3.8</b>	96.6/98.1/ <b>99.5/99.2</b>	96.1/98.2/ <b>99.5/99.3</b>	96.5/98.1/ <b>99.4/98.9</b>
	TINr	11.9/7.6/ <b>2.4/6.3</b>	7.9/6.2/ <b>3.5/5.6</b>	97.1/98.5/ <b>99.5/98.8</b>	96.8/98.6/ <b>99.6/98.8</b>	97.2/98.4/ <b>99.6/98.7</b>
	LSUNc	17.1/12.8/ <b>2.2/5.2</b>	9.7/3.7/ <b>3.0/4.8</b>	95.5/99.4/ <b>99.5/98.7</b>	93.7/99.4/ <b>99.6/98.9</b>	90.4/99.4/ <b>99.5/98.1</b>
	LSUNr	7.2/3.4/ <b>1.3/3.7</b>	6.1/3.8/ <b>2.4/4.3</b>	98.5/99.3/ <b>99.8/99.2</b>	98.5/99.4/ <b>99.8/99.2</b>	94.0/99.3/ <b>99.8/99.0</b>
CIFAR100	TINc	48.1/41.7/ <b>23.4/27.3</b>	22.0/18.9/ <b>11.0/13.2</b>	85.6/88.6/ <b>95.9/94.1</b>	86.8/89.1/ <b>96.2/94.5</b>	83.1/87.0/ <b>95.8/93.5</b>
	TINr	47.2/29.4/ <b>24.4/19.8</b>	22.4/14.2/ <b>9.9/10.3</b>	85.3/93.7/ <b>96.5/96.3</b>	87.0/94.0/ <b>96.4/96.3</b>	82.8/93.8/ <b>96.8/96.3</b>
	LSUNc	50.2/38.8/ <b>32.5/63.2</b>	24.4/13.9/ <b>15.6/29.6</b>	82.3/93.8/ <b>92.4/78.3</b>	85.2/93.6/ <b>93.2/80.0</b>	78.0/93.1/ <b>91.6/76.0</b>
	LSUNr	43.0/20.3/ <b>19.6/20.7</b>	21.1/11.3/ <b>8.6/10.8</b>	86.5/95.7/ <b>97.2/95.8</b>	83.8/96.0/ <b>97.2/96.1</b>	80.6/95.7/ <b>97.3/95.5</b>

Table 1: OOD detection comparison with single-pass methods (top half) and multi-pass inference methods (bottom). Grey background distinguishes our results. Best and second best results are colour coded. Arrows indicate if higher ↑ or lower ↓ values are better. Training objectives (Standard Cross-Entropy, 1D Subspaces, Other) are indicated in brackets next to the method name. HDFF with either a cross-entropy or 1D Subspaces trained model achieves the best performance.

Training Method	ID set	CIFAR10				CIFAR100			
	OOD set	TINc	TINr	LSUNc	LSUNr	TINc	TINr	LSUNc	LSUNr
Other	Counterfactual [29]	0.636	0.635	0.650	0.648	-	-	-	-
	CROSR [45]	0.733	0.763	0.714	0.731	-	-	-	-
	OLTR [24]	0.860	0.852	0.877	0.877	0.746	0.721	0.753	0.747
Standard	Softmax Pred [13]	0.803	0.807	0.794	0.815	0.683	0.683	0.664	0.693
	Max Logit <sup>†</sup> [12]	0.906	0.912	0.897	0.933	0.791	0.789	0.779	0.799
	HDFF (Ours)	<b>0.961</b>	<b>0.944</b>	<b>0.951</b>	<b>0.957</b>	<b>0.869</b>	<b>0.894</b>	0.743	<b>0.890</b>
1D Subspaces [48]	Spectral Disc <sup>†</sup> [48]	0.911	0.920	0.922	0.931	0.794	0.790	<b>0.781</b>	0.802
	HDFF (Ours)	<b>0.959</b>	<b>0.960</b>	<b>0.966</b>	<b>0.972</b>	<b>0.875</b>	<b>0.887</b>	<b>0.834</b>	<b>0.902</b>
MC Sampling Methods (50 Samples)									
Standard	Max Logit [12]	0.915	0.921	0.904	0.940	0.795	0.794	0.782	0.806
	HDFF (Ours)	<b>0.963</b>	<b>0.944</b>	<b>0.952</b>	<b>0.957</b>	<b>0.871</b>	<b>0.896</b>	0.743	<b>0.892</b>
1D Subspaces [48]	Spectral Disc [48]	0.930	0.926	0.894	0.937	0.834	0.863	<b>0.828</b>	0.875
	HDFF (Ours)	<b>0.964</b>	<b>0.965</b>	<b>0.970</b>	<b>0.976</b>	<b>0.890</b>	<b>0.898</b>	<b>0.846</b>	<b>0.913</b>

Table 2: OOD detection comparison by maximum F1-score (↑). Best and second best results are colour coded. Our HDFF detector provides the best F1-score on all benchmarks, except for LSUNc with the cross-entropy DNN.

istics that will be present when OOD samples are observed.

Table 3 quantitatively shows the differences between the ID and OOD datasets through the Battacharyya Coefficient and KL Divergence metrics. This table shows that our method significantly increases separation between ID and OOD data, but also that separation improves for a variety of OOD detection methods when using the 1DS-Model. Importantly, Table 3 presents the argument that both feature-space shaping and monitoring are important aspects to ensure the detection of OOD samples, with the best results coming from the fusion of HDFF and 1D Subspaces.

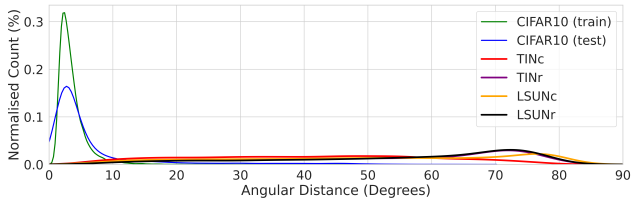
### 5.3. Ablations

#### 5.3.1 Which Layers Are Most Sensitive To OOD Data?

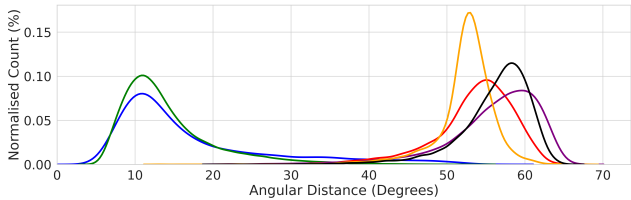
Figure 3 demonstrates the effectiveness of individual layers when they are used in isolation for OOD detection based on our HDFF OOD estimator. Specifically, we see in both ID settings that earlier features in the network appear to be less reliable at detecting OOD samples. This trend is particularly obvious in the CIFAR10 setting where a clear trend upwards as the layer number increases is clear. In the CIFAR100 setting we see that this trend is still present, but

Training Method	Metric	Bhattacharyya Coefficient ↓				KL Divergence ↑			
	OOD Detector	TINc	TINr	LSUNc	LSUNr	TINc	TINr	LSUNc	LSUNr
1D Subspaces [48]	HDFF (Ours)	<b>0.166</b>	<b>0.150</b>	<b>0.164</b>	<b>0.104</b>	<b>8.688</b>	<b>8.479</b>	<b>8.518</b>	<b>9.166</b>
	Spectral Disc [48]	0.405	0.331	0.330	0.285	5.774	6.293	6.408	7.026
	Max Logit [12]	0.325	0.245	0.243	0.186	5.800	6.246	6.306	7.313
Standard	HDFF (Ours)	0.203	0.272	0.269	0.229	8.454	5.321	7.215	6.334
	Spectral Disc [48]	0.404	0.485	0.421	0.419	5.262	3.852	4.916	4.905
	Max Logit [12]	0.476	0.446	0.515	0.341	2.686	2.849	2.284	4.302

Table 3: Quantitative comparison of the separation and similarities of the distributions of angular distance between the CIFAR10 ID set and the OOD sets. Across both training methodologies, our method provides the greatest separation between ID and OOD in the majority of cases.



(a) 1D Subspaces + Spectral Discrepancy

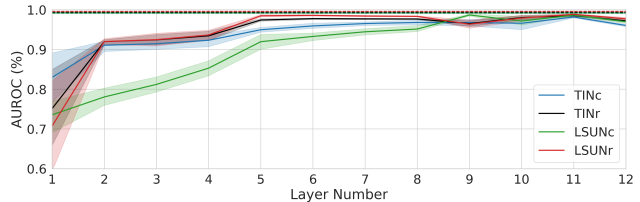


(b) 1D Subspaces + HDFF

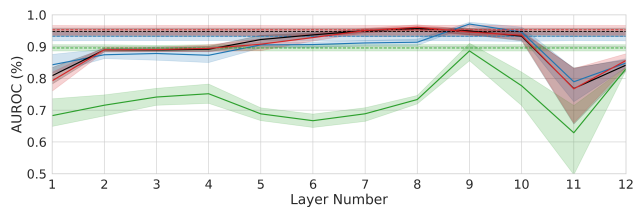
Figure 2: KDE estimate of separation between ID and OOD sets based on minimum angular distance to closest class representative in the CIFAR10 setting. We use a different colour scheme from other plots to help distinguish ID vs OOD. Whilst both methods provide clear separation between ID and OOD set, only HDFF reduces the variance in the distributions of OOD data, giving a more reliable indication of the behaviour of OOD data.

weaker, primarily due to the outlier of LSUNc which only has high performance on layers 9 and 12. This observation confirms suggestions in prior works that shallow layers in a DNN are unable to detect OOD data [35].

The dotted lines, and related 95% confidence shaded area, for each dataset correspond to the fusion of information from all layers; we consider these lines the best that can be reasonably achieved within the bounds of the OOD task. Firstly, in the CIFAR10 setting in Figure 3a we observe that no single individual layer is able to detect the OOD data as well as the fusion of all feature maps. Whilst in the CIFAR100 setting in Figure 3b, we see that the previous observation is sometimes violated, however, this does not indicate a failure of the fusion of feature maps. Criti-



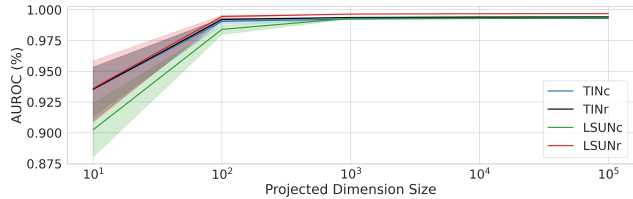
(a) CIFAR10 as In-Distribution



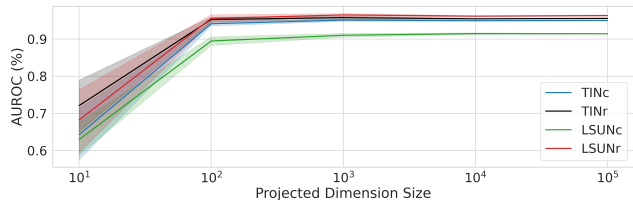
(b) CIFAR100 as In-Distribution

Figure 3: Comparison of effectiveness for OOD detection of each layer individually with the AUROC measure. Mean and 95% confidence interval over 5 randomly initialised models trained with the 1D Subspaces methodology. Dotted lines correspond to the results attained by the fusion of all 12 ResNet Blocks. Performance of individual layers shows a trend toward later layers being more effective at detecting OOD data, with the trend being much stronger in CIFAR10. The fusion of feature maps from across the network provides good general performance across all datasets and does not require calibration on OOD data to set.

cally, we note two points in favour of the fusion of features; (1) Without OOD data the optimal layer combination for a given data set is unknown and (2) The optimal layer combination is not consistent between ID and OOD data configurations. To summarise, note that if there is no access to OOD data at training time to determine which layer(s) are the best then the fusion of feature maps from across the network often provides the best performance or a close approximation. We provide extra ablations against other metrics in the Supplementary Material.



(a) CIFAR10 as In-Distribution



(b) CIFAR100 as In-Distribution

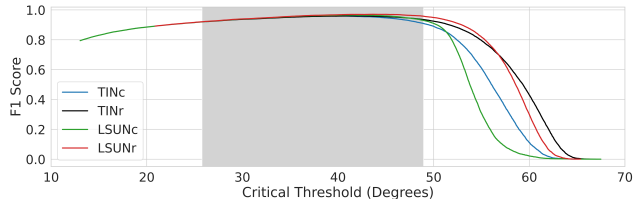
Figure 4: Ablation of the required size of projected HD space to achieve best OOD detection performance. Individual plot lines show mean and 95% confidence interval over 10 independent initialisations of projection matrices on the same model trained with the 1D Subspaces [48] methodology. Features should be projected into a HD space in the range of  $10^3 - 10^4$  dimensions to remove the potential for variation in OOD detection performance.

### 5.3.2 Projection Dimensionality

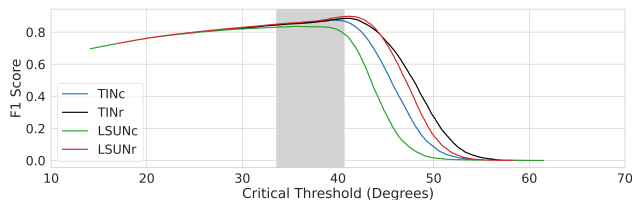
Figure 4 visualises the influence of the number of dimensions in the hyperdimensional space on the OOD detection performance. Specifically, we plot the mean and 95% confidence interval over 10 initialisations of the random projection matrices at each order of magnitude for a single 1D Subspaces [48] trained model. The general trend seen in both figures is that as the number of dimensions increases up to  $10^3$  the mean performance of the HDFS detector increases. Similarly, we see that the bounds of 95% confidence all but effectively disappear when considering spaces of  $10^3$  dimensions or greater. The results of this ablation show that standard choices of hyperdimensional space in the range of  $10^3 - 10^4$  will produce reasonable results, consistent with conventions used in HDC literature [31, 28, 14].

### 5.3.3 Calibration of Critical Threshold

During deployment, it is often more useful to have an OOD detector produce a binarisation of ID vs OOD rather than a raw OOD estimate; the grey regions in Figure 5 show a range of critical thresholds that will produce performance reasonably close to optimal in this setting. Specifically, the grey regions in Figure 5 show a region of confidence where any critical value would produce an F1-score within 5% of the maximum value achieved on each dataset, an approx-



(a) CIFAR10 as In-Distribution



(b) CIFAR100 as In-Distribution

Figure 5: F1-score for binarisation at different critical values of angular distance to closest class descriptor. Model used is the 1D Subspaces trained WRN28-10. The grey region corresponds to binarisations that would produce a result within 5% of the maximum F1-score achieved for that OOD set. The overlap of the grey regions between (a) and (b) indicates that there is a range of critical threshold values between approximately 35 to 41 degrees that will produce reasonable performance in general settings.

imate standard of reasonable performance. As expected, this region is larger in the easier CIFAR10 setting, Figure 5a and narrower on the harder CIFAR100 setting, Figure 5b. The region of overlap between the two Figures provides an indication that a reliable level of performance can be reached with a binarisation value in the range of approximately 35-41 degrees. In practice, additional considerations will need to be made with respect to precision and recall requirements, we use F1-score as a general guide for reliable performance across both metrics.

## 6. Conclusion

This paper introduced the powerful ideas from hyperdimensional computing into the important task of OOD detection. We show that using feature maps extracted from *multiple* layers across the network proves to be critical for detecting OOD samples. We show that when combined with a recent OOD detector we advance the state-of-the-art in OOD detection, leaving less than 1% performance gains to be made on several benchmark configurations. We investigate the sensitivity of individual layers to OOD data and find that the fusion of feature maps provides the best general performance with no requirements for OOD data to fine-tune on. We consider the application of HDC to the feature maps of DNNs to be a promising field for future works. In this paper, we utilised the simple but powerful element-wise

addition for bundling, however, this is one of potentially many applications of HDC to DNNs, opening new future research directions.

## References

- [1] Petra Bevandić, Ivan Krešo, Marin Oršić, and Siniša Šegvić. Simultaneous semantic segmentation and outlier detection in presence of domain shift. In Gernot A. Fink, Simone Frin-trop, and Xiaoyi Jiang, editors, *Pattern Recognition*, pages 33–47, Cham, 2019. Springer International Publishing.
- [2] Hermann Blum, Paul-Edouard Sarlin, Juan Nieto, Roland Siegwart, and Cesar Cadena. The fishyscapes benchmark: Measuring blind spots in semantic segmentation. *International Journal of Computer Vision*, 129(11):3119–3135, Nov 2021.
- [3] Jia Deng, Wei Dong, Richard Socher, Li-Jia Li, Kai Li, and Li Fei-Fei. Imagenet: A large-scale hierarchical image database. In *2009 IEEE conference on computer vision and pattern recognition*, pages 248–255. Ieee, 2009.
- [4] Terrance DeVries and Graham W Taylor. Learning confidence for out-of-distribution detection in neural networks. *arXiv preprint arXiv:1802.04865*, 2018.
- [5] Giancarlo Di Biase, Hermann Blum, Roland Siegwart, and Cesar Cadena. Pixel-wise anomaly detection in complex driving scenes. In *Proceedings of the IEEE/CVF Conference on Computer Vision and Pattern Recognition (CVPR)*, pages 16918–16927, June 2021.
- [6] Yarin Gal and Zoubin Ghahramani. Dropout as a Bayesian approximation: Representing model uncertainty in deep learning. In *Proceedings of the 33rd International Conference on Machine Learning (ICML-16)*, 2016.
- [7] Stephen I. Gallant and T. Wendy Okaywe. Representing Objects, Relations, and Sequences. *Neural Computation*, 25(8):2038–2078, 08 2013.
- [8] R. Gayler. Multiplicative binding, representation operators & analogy. In *Advances in analogy research: Integr. of theory and data from the cogn., comp., and neural sciences*, 1998.
- [9] Lulu Ge and Keshab K. Parhi. Classification using hyperdimensional computing: A review. *IEEE Circuits and Systems Magazine*, 20(2):30–47, 2020.
- [10] Jan Gosmann and Chris Eliasmith. Vector-Derived Transformation Binding: An Improved Binding Operation for Deep Symbol-Like Processing in Neural Networks. *Neural Computation*, 31(5):849–869, 05 2019.
- [11] Matthias Hein, Maksym Andriushchenko, and Julian Bitterwolf. Why relu networks yield high-confidence predictions far away from the training data and how to mitigate the problem. In *Proceedings of the IEEE/CVF Conference on Computer Vision and Pattern Recognition (CVPR)*, June 2019.
- [12] Dan Hendrycks, Steven Basart, Mantas Mazeika, Mohammadreza Mostajabi, Jacob Steinhardt, and Dawn Song. Scaling out-of-distribution detection for real-world settings. *arXiv preprint arXiv:1911.11132*, 2019.
- [13] Dan Hendrycks and Kevin Gimpel. A baseline for detecting misclassified and out-of-distribution examples in neural networks. *Proceedings of International Conference on Learning Representations*, 2017.
- [14] Alejandro Hernández-Cano, Cheng Zhuo, Xunzhao Yin, and Mohsen Imani. *Real-Time and Robust Hyperdimensional Classification*, page 397–402. Association for Computing Machinery, New York, NY, USA, 2021.
- [15] Haiwen Huang, Zhihan Li, Lulu Wang, Sishuo Chen, Bin Dong, and Xinyu Zhou. Feature space singularity for out-of-distribution detection. In *Proceedings of the Workshop on Artificial Intelligence Safety 2021 (SafeAI 2021)*, 2021.
- [16] Pentti Kanerva. Hyperdimensional computing: An introduction to computing in distributed representation with high-dimensional random vectors. *Cognitive Computation*, 1(2):139–159, Jun 2009.
- [17] Brent Komer, Terrence Stewart, Aaron Voelker, and Chris Eliasmith. A neural representation of continuous space using fractional binding. In *CogSci*, pages 2038–2043, 07 2019.
- [18] Alex Krizhevsky and Geoffrey Hinton. Learning multiple layers of features from tiny images. Technical Report 0, University of Toronto, Toronto, Ontario, 2009.
- [19] Balaji Lakshminarayanan, Alexander Pritzel, and Charles Blundell. Simple and scalable predictive uncertainty estimation using deep ensembles. In I. Guyon, U. V. Luxburg, S. Bengio, H. Wallach, R. Fergus, S. Vishwanathan, and R. Garnett, editors, *Advances in Neural Information Processing Systems*, volume 30. Curran Associates, Inc., 2017.
- [20] Kimin Lee, Honglak Lee, Kibok Lee, and Jinwoo Shin. Training confidence-calibrated classifiers for detecting out-of-distribution samples. In *International Conference on Learning Representations*, 2018.
- [21] Kimin Lee, Kibok Lee, Honglak Lee, and Jinwoo Shin. A simple unified framework for detecting out-of-distribution samples and adversarial attacks. In S. Bengio, H. Wallach, H. Larochelle, K. Grauman, N. Cesa-Bianchi, and R. Garnett, editors, *Advances in Neural Information Processing Systems*, volume 31. Curran Associates, Inc., 2018.
- [22] Shiyu Liang, Yixuan Li, and R. Srikant. Enhancing the reliability of out-of-distribution image detection in neural networks. In *International Conference on Learning Representations*, 2018.
- [23] Weitang Liu, Xiaoyun Wang, John Owens, and Yixuan Li. Energy-based out-of-distribution detection. *Advances in Neural Information Processing Systems*, 2020.
- [24] Ziwei Liu, Zhongqi Miao, Xiaohang Zhan, Jiayun Wang, Boqing Gong, and Stella X. Yu. Large-scale long-tailed recognition in an open world. In *IEEE Conference on Computer Vision and Pattern Recognition (CVPR)*, 2019.
- [25] Wesley J Maddox, Pavel Izmailov, Timur Garipov, Dmitry P Vetrov, and Andrew Gordon Wilson. A simple baseline for bayesian uncertainty in deep learning. In H. Wallach, H. Larochelle, A. Beygelzimer, F. d’Alché-Buc, E. Fox, and R. Garnett, editors, *Advances in Neural Information Processing Systems*, volume 32. Curran Associates, Inc., 2019.
- [26] Dimity Miller, Niko Sunderhauf, Michael Milford, and Feras Dayoub. Class anchor clustering: A loss for distance-based open set recognition. In *Proceedings of the IEEE/CVF Winter Conference on Applications of Computer Vision*, pages 3570–3578, 2021.

- [27] Dimity Miller, Niko Sünderhauf, Michael Milford, and Feras Dayoub. Uncertainty for identifying open-set errors in visual object detection. *CoRR*, abs/2104.01328, 2021.
- [28] Justin Morris, Yilun Hao, Roshan Fernando, Mohsen Imani, Baris Aksanli, and Tajana Rosing. Locality-based encoder and model quantization for efficient hyper-dimensional computing. *IEEE Transactions on Computer-Aided Design of Integrated Circuits and Systems*, pages 1–1, 2021.
- [29] Lawrence Neal, Matthew Olson, Xiaoli Fern, Weng-Keen Wong, and Fuxin Li. Open set learning with counterfactual images. In *Proceedings of the European Conference on Computer Vision (ECCV)*, September 2018.
- [30] Peer Neubert, Stefan Schubert, and Peter Protzel. An introduction to hyperdimensional computing for robotics. *KI - Künstliche Intelligenz*, 33(4):319–330, Dec 2019.
- [31] Peer Neubert, Stefan Schubert, Kenny Schlegel, and Peter Protzel. Vector semantic representations as descriptors for visual place recognition. In *Robotics: Science and Systems XVII*. Robotics: Science and Systems Foundation, jul 2021.
- [32] Philipp Oberdiek, Matthias Rottmann, and Gernot A. Fink. Detection and retrieval of out-of-distribution objects in semantic segmentation. In *2020 IEEE/CVF Conference on Computer Vision and Pattern Recognition, CVPR Workshops 2020, Seattle, WA, USA, June 14-19, 2020*, pages 1331–1340. IEEE, 2020.
- [33] Nicolas Papernot and Patrick D. McDaniel. Deep k-nearest neighbors: Towards confident, interpretable and robust deep learning. *CoRR*, abs/1803.04765, 2018.
- [34] Tony Plate. A common framework for distributed representation schemes for compositional structure. In *Connectionist Systems for Knowledge Representation and Deduction*, pages 15–34, July 1997.
- [35] Janis Postels, Hermann Blum, Cesar Cadena, Roland Siegwart, Luc Van Gool, and Federico Tombari. Quantifying aleatoric and epistemic uncertainty using density estimation in latent space. *CoRR*, abs/2012.03082, 2020.
- [36] Abbas Rahimi, Pentti Kanerva, and Jan M. Rabaey. A robust and energy-efficient classifier using brain-inspired hyperdimensional computing. In *Proceedings of the 2016 International Symposium on Low Power Electronics and Design, ISLPED '16*, page 64–69, New York, NY, USA, 2016. Association for Computing Machinery.
- [37] Quazi Marufur Rahman, Niko Sünderhauf, and Feras Dayoub. Online monitoring of object detection performance post-deployment. *CoRR*, abs/2011.07750, 2020.
- [38] Quazi Marufur Rahman, Niko Sünderhauf, and Feras Dayoub. Did you miss the sign? a false negative alarm system for traffic sign detectors. In *2019 IEEE/RSJ International Conference on Intelligent Robots and Systems (IROS)*, pages 3748–3753, 2019.
- [39] Jie Ren, Stanislav Fort, Jeremiah Liu, Abhijit Guha Roy, Shreyas Padhy, and Balaji Lakshminarayanan. A simple fix to mahalanobis distance for improving near-ood detection. *CoRR*, abs/2106.09022, 2021.
- [40] Andrew M. Saxe, James L. McClelland, and Surya Ganguli. Exact solutions to the nonlinear dynamics of learning in deep linear neural networks. In *Yoshua Bengio and Yann LeCun, editors, 2nd International Conference on Learning Representations, ICLR 2014, Banff, AB, Canada, April 14-16, 2014, Conference Track Proceedings*, 2014.
- [41] Kenny Schlegel, Peer Neubert, and Peter Protzel. A comparison of vector symbolic architectures, 2020.
- [42] Paul Smolensky. Tensor product variable binding and the representation of symbolic structures in connectionist systems. *Artificial Intelligence*, 46(1):159–216, 1990.
- [43] Niko Sünderhauf, Oliver Brock, Walter Scheirer, Raia Hadsell, Dieter Fox, Jürgen Leitner, Ben Upcroft, Pieter Abbeel, Wolfram Burgard, Michael Milford, et al. The limits and potentials of deep learning for robotics. *The International Journal of Robotics Research*, 37(4-5):405–420, 2018.
- [44] PyTorchLightning Team. Torchmetrics: Machine learning metrics for distributed, scalable pytorch applications. <https://github.com/PyTorchLightning/metrics>, 2020.
- [45] Ryota Yoshihashi, Wen Shao, Rei Kawakami, Shaodi You, Makoto Iida, and Takeshi Naemura. Classification-reconstruction learning for open-set recognition. In *Proceedings of the IEEE/CVF Conference on Computer Vision and Pattern Recognition (CVPR)*, June 2019.
- [46] Fisher Yu, Yinda Zhang, Shuran Song, Ari Seff, and Jianxiong Xiao. Lsun: Construction of a large-scale image dataset using deep learning with humans in the loop. *arXiv preprint arXiv:1506.03365*, 2015.
- [47] Qing Yu and Kiyoharu Aizawa. Unsupervised out-of-distribution detection by maximum classifier discrepancy. In *Proceedings of the IEEE/CVF International Conference on Computer Vision (ICCV)*, October 2019.
- [48] Alireza Zaeemzadeh, Niccolo Bisagno, Zeno Sambugaro, Nicola Conci, Nazanin Rahnavard, and Mubarak Shah. Out-of-distribution detection using union of 1-dimensional subspaces. In *Proceedings of the IEEE/CVF Conference on Computer Vision and Pattern Recognition (CVPR)*, pages 9452–9461, June 2021.
- [49] Sergey Zagoruyko and Nikos Komodakis. Wide residual networks. *CoRR*, abs/1605.07146, 2016.
- [50] Arthur Zimek, Erich Schubert, and Hans-Peter Kriegel. A survey on unsupervised outlier detection in high-dimensional numerical data. *Stat. Anal. Data Min.*, 5(5):363–387, Oct. 2012.

## A. Supplementary Experiments

We provide additional experiments that show the robustness of HDFF, ablates minor components, highlights interesting phenomena and adds additional context to experiments shown in the main paper.

### A.1. Variation over Model Initialisations

Table 4 shows the range of AUROC values for independent random model weight initialisations for the 1D Subspaces model [48] over 5 models. The same 5 models are shared between the HDFF and Spectral Discrepancy [48] detectors for a fair comparison. Across every ID + OOD dataset configuration it is clear that HDFF vastly improves upon the performance of the 1D Subspaces model. Similarly, we see in all of the CIFAR10 setting and the resized CIFAR100 setting that we also reduce the potential for variation in performance of different model initialisations. The results from Table 4 shows directly that HDFF consistently improves upon the already high performing Spectral Discrepancy detector irrespective of model initialisations.

### A.2. Similarity of Class Bundles

Figure 6 shows the cosine similarity of the class-representatives, hyperdimensional bundled vectors for HDFF in Figures 6a and 6b, and first singular vectors for the Spectral Discrepancy detector [48] in Figures 6c and 6d. For Figures 6c and 6d we show the absolute value of the cosine similarity between singular vectors as the original spectral discrepancy detector uses the absolute cosine similarity for OOD scoring. It is clear to see that for both tasks, in particular the CIFAR100 task, that the class-representatives for the Spectral Discrepancy detector are significantly more dissimilar, behaviour that the 1D Sub-

ID set	OOD set	HDFF	Spectral Disc [48]
CIFAR10	TINc	<b>99.15 ± 0.17</b>	95.84 ± 0.62
	TINr	<b>99.36 ± 0.08</b>	97.28 ± 0.61
	LSUNc	<b>99.19 ± 0.15</b>	96.66 ± 0.62
	LSUNr	<b>99.58 ± 0.10</b>	97.63 ± 0.62
CIFAR100	TINc	<b>92.79 ± 2.24</b>	84.39 ± 2.23
	TINr	<b>93.97 ± 2.18</b>	83.75 ± 3.30
	LSUNc	<b>89.77 ± 1.68</b>	82.54 ± 0.87
	LSUNr	<b>94.60 ± 2.46</b>	85.58 ± 3.68

Table 4: Range of values in the AUROC metric over 5 random initialisations of models trained with the 1D Subspaces objective. The same 5 models are shared between the HDFF and Spectral Disc OOD detectors. **Best** per ID + OOD dataset configuration is coloured. In all cases, no matter the initialisation of the 1D Subspaces model, our HDFF detector significantly improves performance over the Spectral Discrepancy detector.

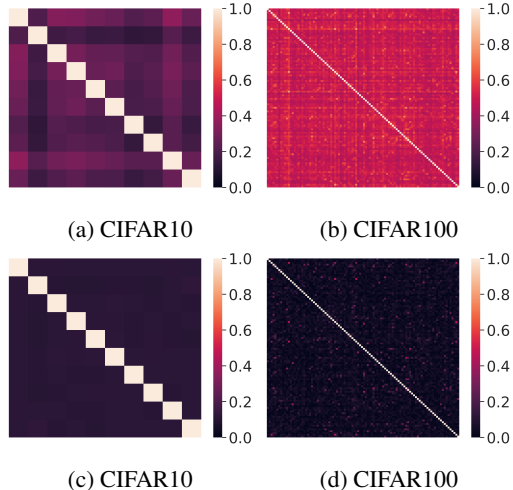


Figure 6: Cosine similarity of class representatives for a 1D Subspaces trained model from the HDFF and Spectral Discrepancy detectors. (a) and (b) Hyperdimensional bundled class-specific vectors from HDFF. (c) and (d) class-specific singular vectors for spectral discrepancy detector. Despite being applied to the exact same model, we see that there is far more inter-class similarities between the feature maps than the final feature layer of the network.

spaces objective specifically optimises for. This behaviour was expected, however, this highlights an important question for future work; for the out-of-distribution task, is allowing for some inter-class similarity desirable or is the complete orthogonalisation of class representatives desirable? We leave this open for potential future work.

Importantly, we note that the model used to produce all of these figures was the 1DS-Model with the modified training pipeline of unfreezing the weights and biases during training. Figures 6c and 6d shows that these modifications have not fundamentally changed the behaviour of the 1D Subspaces training methodology as all of the singular vectors are still orthogonal or near-orthogonal to each other.

### A.3. Preprocessing

In order to apply our hyperdimensional feature fusion to the feature maps of a DNN we first implemented a preprocessing pipeline that made use of a global pooling operation and mean-centering. Table 5 ablates these components, showing their influence to the overall results described in the main paper.

Table 5 offers us two core findings; firstly, mean-centering provides performance increases in every scenario, although in the max pooling CIFAR10 setting, these improvements are minute. Secondly, the use of max pooling improves the results of the HDFF detector over average pooling in the majority of circumstances. The use of

max pooling differs from our implementation in the main paper as the effectiveness of using the max pooling operation over the average pooling operation was discovered after submission of the main paper to this conference. We do note however, that using these results to motivate the use of max pooling could be considered a minor form of calibrating on OOD data since the effectiveness of max pooling cannot be known prior to receiving results for the OOD task. This does not hold true for mean-centering, which is well-known and commonly used methodology that is general considered good practice.

#### A.4. Additional Layer Ablations

Figure 7 provides additional ablations of individual layer performance with respect to the other standard metrics for the benchmark defined in [22]; those being FPR@95, Detection Error and Maximum F1 Score. Ablations for the AUPR-In and AUPR-Out metrics were not included as they are a near-identical match to the AUROC study provided in the main paper. Across both settings we see that the cropped datasets nearly perfectly mirror each other, indicating that there is a set of features that HDFS is consistently strong at detecting. In the CIFAR10 setting we see that across all metrics, there is no individual layer that performs at or above the level of the the fusion of feature maps. This trend is violated by the later layers, 7 through to 9 in the CIFAR100 setting. In particular, we see that the metrics that measure binarised performance, F1 and FPR@95, appear to have the largest increase above the fusion of fea-

tures, usually in only a single layer. Overall, we make the same observation as in the main paper; there is no individual layer that performs well across all OOD datasets, assuming we already have the prior knowledge of how well each layer performs at this task. Future work into weighting individual layers based on predicted performance may be an important consideration.

ID set	OOD set	Centering	Avg Pool	Max Pool
CIFAR10	TINc	✓	99.2	<b>99.5</b>
		✗	98.7	<b>99.5</b>
	TINr	✓	99.4	<b>99.7</b>
		✗	99.3	<b>99.7</b>
LSUNc	✓	99.3	<b>99.5</b>	
	✗	98.9	<b>99.5</b>	
LSUNr	✓	99.7	<b>99.9</b>	
	✗	99.5	<b>99.9</b>	
CIFAR100	TINc	✓	<b>95.0</b>	94.1
		✗	91.6	93.0
	TINr	✓	<b>95.8</b>	95.6
		✗	95.0	94.7
LSUNc	✓	91.4	<b>93.1</b>	
	✗	86.8	92.3	
LSUNr	✓	96.5	<b>96.6</b>	
	✗	96.0	95.7	

Table 5: Ablation of our feature preprocessing in terms of the AUROC metric in the single-inference pass setting with the 1D Subspaces trained model. **Best** result per ID + OOD dataset combination is coloured. Across the majority of the configurations, max pooling with mean-centering provides to best overall AUROC scores.

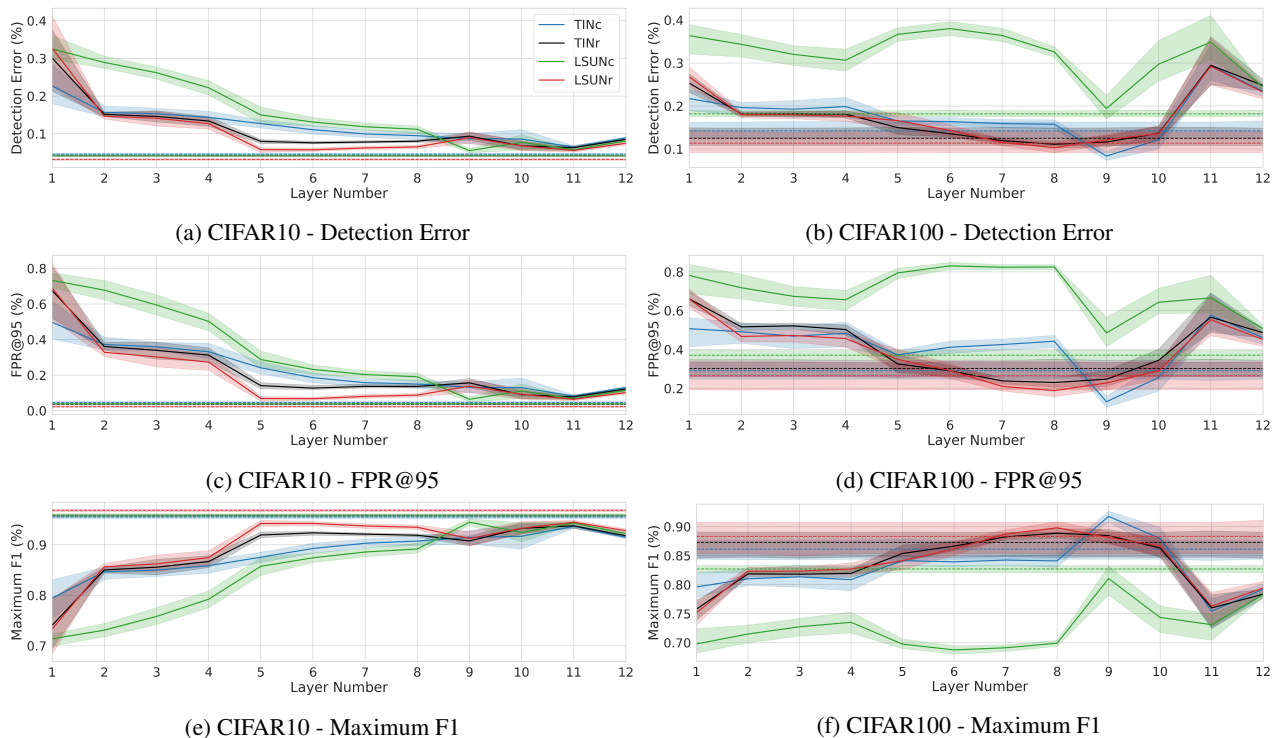


Figure 7: Layer-wise ablation across multiple metrics for the 1D Subspaces trained model. We plot mean and 95% confidence interval for each datasets with the dotted lines corresponding to the performance of the fusion of feature maps across the network. For the CIFAR10 setting in (a), (c) and (e) it is clear that the fusion of feature maps from across the network provide the best performance. For the CIFAR100 setting in (b), (d) and (f) we see that violations of this characteristic are present in the later layers of 7, 8 and 9. Although some individual layers violate this characteristic, we note that no individual layer performs well across all of the OOD datasets.